Applied Catalysis B: Environmental 254 (2019) 569–579

Contents lists available at ScienceDirect

Applied Catalysis B: Environmental

journal homepage: www.elsevier.com/locate/apcatb

Catalytic ozonation benefit from the enhancement of electron transfer by the coupling of g-C_3N_4 and $LaCoO_3$: Discussion on catalyst fabrication and electron transfer pathway

Yuting Zhang[a], Qingwei Li[a], Yujin Long[a], Jiawei Zou[a], Zilong Song[a], Chao Liu[a], Longyan Liu[a], Fei Qi[a,*], Bingbing Xu[b], Zhonglin Chen[c,**]

[a] Beijing Key Lab for Source Control Technology of Water Pollution, College of Environmental Science and Engineering, Beijing Forestry University, Beijing 100083, PR China
[b] State Key Laboratory of Environmental Criteria and Risk Assessment, Chinese Research Academy of Environmental Sciences, Beijing 100012, PR China
[c] State Key Laboratory of Urban Water Resource and Environment, Harbin Institute of Technology, Harbin 150090, PR China

ARTICLE INFO

Keywords:
Catalytic ozonation
Electron transfer
g-C_3N_4
$LaCoO_3$

ABSTRACT

In this study, the novel design approach of catalyst in catalytic ozonation was proposed to enhance electron transfer in catalytic ozonation, achieving a better performance on micro-pollutants degradation and bromate elimination. The combination of perovskite oxide ($LaCoO_3$, LCO) and graphitic carbon nitride (g-C_3N_4, CN) was studied to overcome some significant drawbacks of catalytic ozonation with metal oxides catalysts, such as the rate-limiting step between Me^{n+} and $Me^{(n+m)+}$. Additionally, the in-depth analysis of electron transfer pathway in CN/LCO catalytic ozonation was provided, which provided new insight into the design of highly efficient catalysts for facilitating micro-pollutants degradation and bromate inhibition. CN/LCO was successfully prepared and connected by the formation of -C-O-Co linkages, which exhibited a high activity in the catalytic ozonation for the synchronous degradation of benzotriazole (BZA) and elimination of bromate. Interestingly, being different with the general mechanism of catalytic ozonation, nitrogen vacancies and -C-O-Co bonds were the main active sites in CN/LCO rather than the surface hydroxyl group. With the largest amount of -C-O-Co and more nitrogen defects, CN/LCO exhibited a fast charge transfer along the in-plane direction. Additionally, the fast reduction of Co^{3+} to Co^{2+} was found to be initialized by $O_2^{\bullet-}$ and single electrons in catalytic ozonation, which resulted in more formation of H_2O_2 and good inhibition efficiency of bromate. This study not only present the good catalytic ozonation ability for refractory organic micro-pollutants and elimination of bromate using CN/LCO, but also provided insight into electron transfer pathway in the interlayers of CN/LCO, which will be significant for the design of catalyst and to promote charge transfer in catalytic ozonation.

1. Introduction

Organic contaminants in soils [1], surface water [2], ground water [3] and secondary effluents of municipal wastewater [4] have achieved much concerns. Most of contaminants are harmful even at low concentrations [5] due to the high toxicity. In recent years, many efficient catalysts have been used to enhance oxidation ability of contaminants during ozonation that is able to removal organisms in the aquatic environment [6–8]. Metal oxides and metal oxide-based composites are used as important catalysts in catalytic ozonation [1]. Various kinds of metal oxides, such as MnO_2 [2], ZnO [3], CuO [4], Fe_2O_3 [1], Co_3O_4 [5], TiO_2 [6] and γ-Al_2O_3 [7], have been used to enhance the performance of the sole ozonation in drinking water and wastewater treatment, to overcome the drawbacks of the sole ozonation, such as lower ozone decomposition activity, energy consumption and selective oxidation of the molecular ozone [8]. However, a weakness of metal oxide catalytic ozonation is the cycle reaction between Me^{n+} and $Me^{(n+m)+}$ over the surface of metal oxide, as the main rate-limiting step [9].

As the hotspot, layered-structure carbon materials (such as graphene oxide (GO) [10], reduced GO (rGO) [11] and graphitic carbon nitride (g-C_3N_4, CN) and carbon composites have been successfully applied as photocatalysts [12–14] and Fenton-like catalysts [15,16]. It has been reported that these catalysts can enhance catalytic ability to

* Corresponding author.
** Co-corresponding author.
E-mail addresses: qifei@bjfu.edu.cn (F. Qi), zhonglinchen@hit.edu.cn (Z. Chen).

https://doi.org/10.1016/j.apcatb.2019.05.019
Received 22 February 2019; Received in revised form 27 April 2019; Accepted 4 May 2019
Available online 07 May 2019
0926-3373/

destruct bacterial [12,14], degrade acyclovir [11], removal Acid Red 73 [16], 2-chlorphenol, bisphenol A [15] and so on. The large surface area, good conductive ability, defective structure and increasing active sites may enhance catalytic performance [14]. Recently, layered-structure carbon materials have been also applied to catalytic ozonation [10] and above advantages made the possibility of application of these kind of catalysts in catalytic ozonation. Results showed that the presence of an intrinsic defective structure and surface oxygen-containing groups of the layered-structure carbon materials contributed to the catalytic ozone decomposition and achieved a higher performance for the degradation of refractory organics [11]. Unfortunately, the instability of GO was found in catalytic ozonation [10]. Therefore, CN with highly stable chemical and thermal features owing to the strong covalent bonds, was proposed to serve as a catalyst or supporter in the catalytic ozonation. Song et al. reported that CN showed a better activity in the catalytic ozonation for the degradation of 4-chlorobenzoic acid (*p*-CBA) and benzotriazole (BZA) [10]. However, Xiao et al. reported that CN showed no activity for the degradation of oxalic acid by catalytic ozonation. Yuan et al. reported that atrazine (ATZ) removal was enhanced by oxygen functionalized CN catalytic ozonation due to the novel electronic properties and additional active sites [17]. Additionally, chemical doping of metal ions into the framework of CN to form a composite as catalytic centers, modified the surface properties of CN and rearranged the electron distribution, which might promote the electron charge transfer or create more active sites in catalytic ozonation [18]. Zero-valent zinc/CN was used to remove atrazine by catalytic ozonation, due to the large surface area and fast electron transfer of CN [19]. The enhancement efficiency was achieved by the coupling of ZnO and CN for atrazine degradation owing to the surface electronic and pore structures [18].

However, an in-depth understanding of the electron transfer pathway in catalytic ozonation (e.g., in the interlayers of layered-structure carbon materials and between metal ions and layered-structure carbon materials) is still unclear. Furthermore, the above studies only focused on the ability for micro-contaminants degradation but ignored the formation of toxic bromate (BrO_3^-).

BZA, a kind of ultraviolet absorbents, was widely used in extensive fields, which led to its significant release into the water environment and harmed to the ecological environment and human health [20]. The occurrence of BZA in surface water, ground water and primary/secondary effluents of municipal wastewater has been reported [21]. The detected [BZA] in surface water was 3.4 μg/L [21], much higher [BZA] was found in groundwater from airport, up to 126 mg/L owe to the heavily use of antifogging agent [22]. And the varied [BZA] was observed in primary/secondary effluents of municipal wastewater that from 10 to 100 μg/L [22]. Therefore, it is necessary to develop an effective technique to degrade BZA in the aquatic environment due to its long-term adversary effects [23]. In our previous study, $LaCoO_3$ (LCO) showed better performances for the degradation of benzotriazole (BZA) and elimination of BrO_3^- in catalytic ozonation [24], but the cycle reaction between Co^{2+} and Co^{3+} was the rate-limiting step. Therefore, a combination of CN and LCO (CN/LCO) was used to enhance the electron transfer that resulted in synchronously facilitating BZA degradation and BrO_3^- elimination. The present study provides new insight into the design of high efficient catalyst to facilitate charge transfer and to provide more active sites due to structure and electronic properties in catalytic ozonation, which is not only of scientific significance for a comprehensive understanding of CN-based-metal oxide composites, but also technically important for the design of efficient catalyst in catalytic ozonation.

2. Materials and methods

2.1. CN/LCO fabrication and characterization

The novel CN/LCO was fabricated in two steps. First, LCO was synthesized by a sol-gel method according to a previous study [24]. Then, urea (0.5–3.0 g) as precursor of CN and LCO (0.5 g) were dissolved in DD water (10 mL) with stirring of 6 h. The obtained solution was then dried overnight at 85 °C. The solid composite precursors were placed in a semi-closed alumina crucible with a cover and heated to 350–550 °C at a heating rate of 10 °C/min in a muffle furnace, which was held on for 2 h [25]. After the thermal treatment and natural cooling, the resulting products were collected for further use, and the definitions of the catalysts are shown in Table S1.

The crystal structure of obtained CN/LCO was examined by X-ray diffraction (XRD) (XRD-7000, Shimadzu, Japan). Fourier transform infrared (FT-IR) spectroscopy of the sample was recorded on a spectrometer (VERTEX 70, Bruker, Germany). Raman spectra were measured using an ISA argon-ion laser Raman spectrometer (LabRAM-HR800, Horiba Jobin Yvon, France). High resolution transmission electron microscopy (HR-TEM) images were obtained by a microscope (JEOL, JEM-2010, Japan). Specific surface areas were calculated according to the Brunauer-Emmett-Teller (BET) equation from N_2 adsorption-desorption isotherm data and pore size was calculated by Barrett-Joyner-Halenda (BJH) method (3H-2000PS1, Bulider, China). X-ray photoelectron spectroscopy (XPS) characterization was performed on an ESCALAB MK-2 spectrometer (VG, UK). Electrochemical impedance spectroscopy (EIS) was carried out in a conventional three-electrode cell using a CHI 660E electrochemical workstation (CHI, Shanghai, China), details are shown in Text S1.

2.2. Catalytic ozonation procedure and analysis method

All ozonation tests were conducted in a semi-continuous mode with a standard laboratory ozonizer (3S-A5, Beijing Tonglin Gaoke Technology, Bejing, China) in a 500-mL glass reactor at room temperature, and detailed information is shown in Text S2. The analytical methods for determining [BZA], [TOC], [BrO_3^-], [Br^-], dissolved ozone concentration, [H_2O_2] and [HOBr/OBr^-] are provided in Text S3. Intermediates formed from BZA degradation were identified by liquid chromatography-quadrupole time-of-flight mass spectrometry (LC-Q-TOF-MS) (Text S4) and the formed reactive oxygen species of free radicals (HO· and $O_2{\cdot}^-$) and $^1O_2$ are described in Text S5.

3. Results and discussion

3.1. Effect of calcination temperature on the structure of CN/LCO and its performance

Fig. 1(A) shows XRD patterns of CN/LCO composites fabricated under different calcination temperatures. XRD peaks of LCO were assigned mainly to a rhombohedral structure (JCPDS No. 48-0123) [26], with no impurity peaks. CN showed a distinct peak at 27.6° with typical interlayer-stacking (002) and an in-plane (100) peak at 13.0° (JCPDS card no. 87-1526) [27]. Notably, after the combination of LCO and CN, peaks intensity of LCO decreased significantly, especially for samples obtained under lower calcination temperatures (350 and 400 °C). This may be due to the re-calcination of LCO or structure variation of LCO after the addition of CN. The effect of re-calcination showed very slight effect on the crystal structure of LCO (Fig. S1(A)). Therefore, the addition of CN changed the structure of LCO. Owing to the small dose amount of urea, typical diffraction peaks of CN were absent in the obtained composites. A similar result was also observed in $LaFeO_3$/g-C_3N_4 [28].

From FT-IR result (Fig. 1(B)), peak intensities of CN (810 cm^{-1} of tri-s-triazine units, 1200–1700 cm^{-1} of C—N heterocycles, 3000–3300 cm^{-1} of amines [25]) decreased with an increasing calcination temperature and the above peaks were only observed in samples calcinated at 350 and 400 °C. Hence, a higher temperature calcination decomposed the structure of CN, which was also reported before [29]. Moreover, the Co-O bond peaks (570 and 640 cm^{-1} [30]) decreased

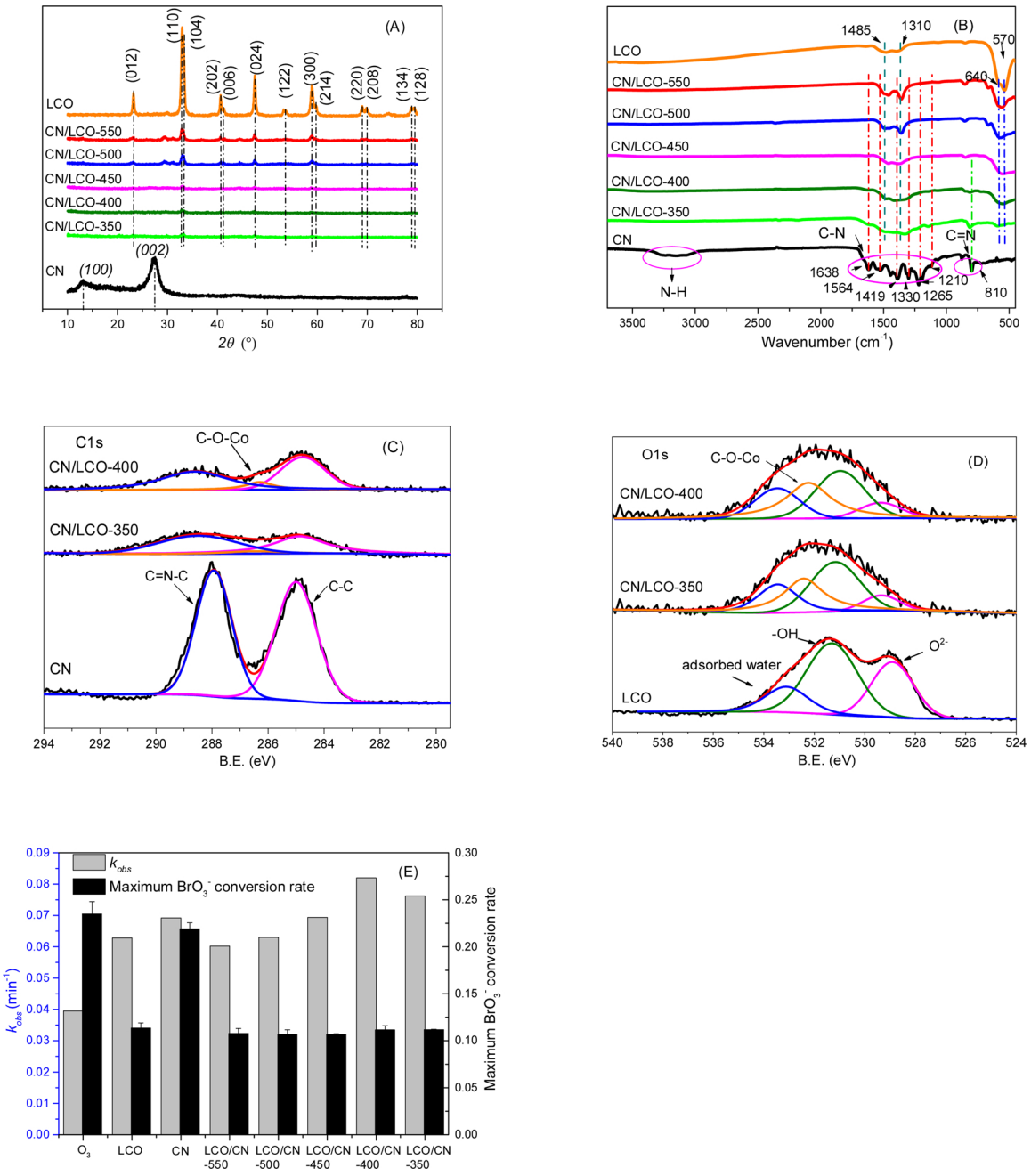

Fig. 1. XRD patterns of CN/LCO with different calcination temperatures (A); FT-IR spectrum of CN/LCO with different calcination temperatures (B); XPS spectrum of C-(C) and O-(D); Degradation performance of benzotriazole and bromate elimination with different calcination temperatures of catalysts (E). Reaction Condition: [Br^-] = 100 μg/L, [O_3] = 1.0 mg/L, [BZA] = 10 mg/L, [catalyst] = 0.25 g/L.

dramatically after the calcination, especially for samples obtained at the lower calcination temperatures (350 and 400 °C), while almost no variation was observed for La-O bond peaks (1310 and 1485 cm^{-1}) [31]. The decrease of the peak intensity of Co-O stretch in CN/LCO might be due to the structure combination of CN and LCO derived from the bonding with a cobalt atom rather than a lanthanum one, because no variation of Co-O or La-O bond was observed after the re-calcination (Fig. S1(B)). Additionally, compared with CN, a significant blue-shift was observed for the peak at 810 cm^{-1} (tri-s-triazine units) in CN/LCO sample. This suggested that the amount of hydrogen bonds in the CN structure decreased, which would promote the transport of charge carriers within the layer of carbon nitride [32], this was more significant for CN/LCO-400.

To confirm the interaction between LCO and CN, C 1s, O 1s, Co 2p and N 1s XPS spectrums were studied (Text S6 and Table S2). After the composition, the intensity of the C═N−C− bond peak (288.7 eV [33]) decreased, especially for CN/LCO-400 (Fig. 1(C) and Table S2). This suggested that the structure of CN was destroyed after the combination. Moreover, new peaks were found in both C 1s (286.5 eV [9]) and O 1s spectrums (532.5 eV [15]) of CN/LCO (Fig. 1(C) and (D)), which were ascribed to a cobalt atom bonding to deprotonated hydroxyl groups through a -C-O-Co bonding bridge [15]. After the combination of CN and LCO, Co $2p_{3/2}$ and Co $2p_{1/2}$ were all obviously shifted (Fig. S1(C)), suggesting that LCO interacted strongly with CN and the bridge was confirmed by the observed -C-O-Co bond. The greater blue-shift of the cobalt species was observed in CN/LCO-400 (0.7 eV) than that in CN/LCO-350 (0.5 eV), which indicated that the interaction of LCO and CN was more significant in CN/LCO-400.

Additionally, CN/LCO-400 showed higher nitrogen vacancies as a higher C/N ratio obtained from the N 1s spectrum (description shown in Fig. S1(D) and Table S2). This was able to explain the coupling of CN and LCO that destroyed the structure of C═N−C− in CN, through the generation of an emerging -C-O-Co bond. The lowest relative content of C═N−C− (Table S2) in CN/LCO-400 also supported the formation of the -C-O-Co bond, which was in accordance with the result of C 1 spectrum.

The coupling of CN and LCO showed higher ratio of I_D/I_G and higher defective degree, which was more significant for CN/LCO-400 (Text S7, Fig. S2 and Table S3), according to Raman spectrum. This result also indirectly confirmed the new bond formation and the destruction of the C═N−C− structure. In summary, CN/LCO prepared herein, was not simply by the mechanical mixing, but by an emerging chemical combination through a -C-O-Co bond. This might result in more structural defects and delocalization electrons, which would be beneficial for electron transfer in catalytic ozonation.

The performance of the prepared CN/LCO on BZA degradation and elimination of BrO_3^- was evaluated (Fig. 1(E)). The observed rate constant (k_{obs}) of BZA degradation by CN/LCO catalytic ozonation showed an increasing tendency (Fig. S3(A)), followed by a decreasing trend with the increasing of the calcination temperature from 350 to 550 °C and the highest BZA removal efficiency was observed when CN/LCO-400 was used (k_{obs} was 0.0820 min^{-1}). Similar results were also observed for TOC removal efficiency (Fig. S3(B)). All the obtained CN/LCO showed remarkable elimination of BrO_3^- formation (Fig. S3(C)) and the maximum inhibition efficiency of BrO_3^- was around 66.2% (Fig. S3(C)). CN/LCO-400 showed the significantly exhibition ability on BrO_3^- generation and 66.6% BrO_3^- was inhibited after 90 min (Fig. S3(C)).

In summary, a better degradation efficiency of BZA and elimination ability on BrO_3^- were observed in CN/LCO-400 catalytic ozonation, which indicated that the optimal calcination temperature was 400 °C and CN/LCO-400 was chosen for the following analysis.

3.2. Effect of precursor amount on the structure of CN/LCO and its performance

There were no obvious typical diffraction peaks of CN in CN/LCO samples, even with different precursor qualities of urea (Fig. 2(A)), because CN precursor dose was too low. However, as the dose of urea was increased, FT-IR peak intensities of C—N heterocycle (1200–1700 cm^{-1}) and tri-s-triazine unit (810 cm^{-1}) increased (Fig. 2(B)), which suggested that more CN was presence in composites. The corresponding diffraction peaks of LCO decreased notably with the increasing urea dose (Fig. 2(A)). Similarly, it was also found that the intensity of Co-O bond peaks (570 and 640 cm^{-1}) decreased dramatically with the increasing urea dose (Fig. 2(B)). The proposed reasons for this observation were as follows: (1) the increasing of CN under higher urea doses covered the surface of LCO; (2) a strong interaction between CN and LCO, due to the formation of -C-O-Co that destroyed LCO structure under higher precursor doses.

According HR-TEM images (Fig. 2(C–E)), LCO attached to the layer CN sheets with smooth surfaces in 1.5-CN/LCO. Additionally, CN sheets were on the edge of the composites, which was similar with the images previously presented in the literature [28]. Interestingly, a multi-layered structure was observed with decrease of the urea mass to 1.0 and 0.5 g, especially for 0.5-CN/LCO, which showed different morphology with the reported g-C_3N_4/TiO_2 that g-C_3N_4 wrapped on the TiO_2 spheres [12]. Elements of La, Co, O, C and N (insets in Fig. 2 (D) and (E)) showed uniform distribution in 1.0-CN/LCO and 0.5-CN/LCO (Fig. S4). At the lower urea doses, LCO was closely adhered to CN sheets and two phases of CN and LCO were in close contact to form an interface, which was beneficial for the formation of -C-O-Co bonds in 0.5-CN/LCO. Being different, elements of La, Co, O were distributed inside in 1.5-CN/LCO, while C and N elements were on the edge (inset in Fig. 2(C)). Then, CN and LCO were separated at the increasing dose of urea (1.5-CN/LCO) and a larger formation of layered-structure CN covered the surface of LCO with the increasing of precursor dose.

The parameters of surface physicals structure of the prepared 0.5-CN/LCO is shown in Table 1. The specific BET surface area of LCO and CN were 15.8 and 63.5 m^2/g, respectively. After the combination, the specific BET surface area of 0.5-CN/LCO was 32.8 m^2/g, which was 2.1 times higher than that of LCO. The increase surface area of the combination of LCO and CN was beneficial for increasing the active sites, which may improve catalytic activity [34]. Meanwhile, the decrease of pore volume or pore diameters of 0.5-CN/LCO may be due to the doping of cobalt ions with CN through chemical binding [18].

The effect of the precursor dose on the catalytic ozonation performance for the degradation of BZA and elimination of BrO_3^- was investigated (Fig. 2(F)). The value of k_{obs} increased and then decreased with the increasing urea dose and a maximum value (0.094 min^{-1}) (Fig. S5(A)) was obtained when the urea dose was 0.5 g (0.5-CN/LCO). Compared with perovskite-type oxides (shown in Table S4), 0.5-CN/LCO showed a significant improvement on the contaminant degradation. The performance of 0.5-CN/LCO was excellent compared with the reported $LaTi_{0.15}Cu_{0.85}O_3$ and $LaTi_{0.15}Co_{0.85}O_3$ [35] using normalized k_{obs}. Similarly, 0.5-CN/LCO also showed the best performance for BZA mineralization (Fig. S5(B)).

The formation of BrO_3^- was promoted with an increasing urea dose and a better elimination of BrO_3^- was achieved when 0.5-CN/LCO was used (Fig. S5(C)). 0.5-CN/LCO showed the highest elimination rate of BrO_3^-, compared with the other previously reported catalysts (Table S4).

In summary, the optimal urea dose was 0.5 g and this value was selected for further study, based on above detailed study. Additionally, effects of reaction parameters, including ozone dose, catalyst dosage, BZA concentrations and initial solution pH, on the performance of catalytic ozonation with 0.5-CN/LCO are provided in Text S8, Fig.s S(6) and S(7).

3.3. Degradation pathway of BZA

Degradation intermediates of BZA in 0.5-CN/LCO catalytic ozonation were analyzed by LC-Q-TOF-MS and a potential degradation pathway is proposed in Fig. 3. The information of the fragment ions (m/z), detected molecular formula and other information are provided in Fig. S8 and Table S5, where six intermediates were firstly reported shown in red in this field. Three main degradation pathways are proposed.

Pathway A, an electrophilic addition reaction between the benzo-moiety of BZA and the molecular ozone formed primary ozonide (C1) [36] that was attacked by the molecular ozone or HO· to form C2 by the ring opening [36]. With further ozonation, C3 with two aldehyde groups was formed rapidly [36]. C4, which lost two carbons, formed with the attack of molecular ozone or HO·. Aldehyde groups in C4 were further oxidized to carboxyl groups (C5 and C6) by the molecular ozone or HO·.

Pathway B, the hydroxylation stages and the electrophilic substitution on a benzene ring [37] were identified as the formation of C7. A second hydroxylation stage led to the formation of C8 that was also substituted by HO· to form C9 in the third hydroxylation stage [38]. The formation of C10, with a carboxyl and an aldehyde group, confirming the derivation and benzene ring opening. Meanwhile, the attack of C9 by molecular ozone or HO· led to a carbon being lost [38] and the formation of aldehyde compound C11. Additionally, two isomers (C12 and C13) formed through the HO· substituted of C8. Compounds with an aldehyde or carboxyl group (C10 and C11) were generated, owing to the oxidation of the molecular ozone and HO·. The loss of a carbon from C10 or oxidation of an aldehyde group from C11 formed C14 with a carboxyl group. Carboxylic acid compound C15 was generated from the oxidation of C13 and C12. Interestingly, a series of intermediates of

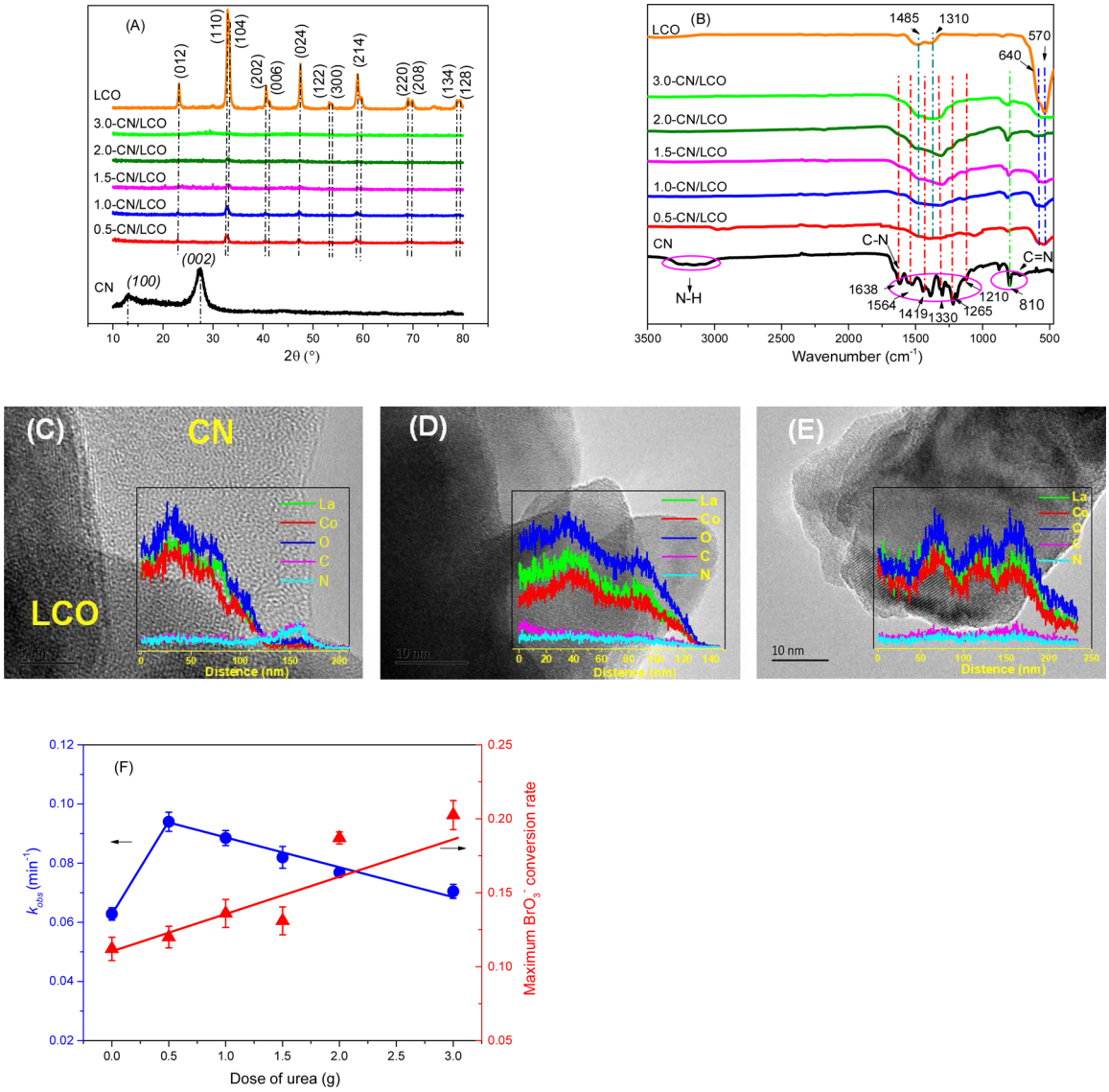

Fig. 2. XRD patterns of CN/LCO with different dose of precursor urea (A); FT-IR spectrum of CN/LCO with different qualities of precursor urea (B); HR-TEM image with EDS mapping (inset in the images) of 1.5-CN/LCO (C), 1.0-CN/LCO (D), 0.5-CN/LCO (E); Effects of the precursor urea dose on the BZA degradation efficiency and on formation of BrO_3^- (F).
Reaction Condition: [Br^-] = 100 μg/L, [O_3] = 1.0 mg/L, [BZA] = 10 mg/L, [catalyst] = 0.25 g/L.

Table 1
Parameters of surface physicals structure of investigating catalyst.

Catalyst	BET surface area (m^2/g)	Total pore volume (mL/g)	Diameters of pore (nm)
LCO	15.8	0.10	24.7
CN	63.5	0.78	49.3
0.5-CN/LCO	32.8	0.12	14.6

BZA were identified firstly. A triazole ring-opening at atom N8, identified as the active site to be attracted [23], led to the formation of C20 and C16. Subsequently, HO· or molecular ozone attack was able to open the benzene ring to form C17 or to form carboxylic acid compounds (C21 and C22).

Pathway C, the oxidation of BZA released N8 that was with abundant charge and no steric hindrance [23] to form C18 with an amino group and a nitro group. Then, a new intermediate (C19) with the benzene ring-opening derived from C18 was identified. The further oxidation by O_3/HO· led to the formation of C16, C17 and carboxylic acid compounds (C21 and C22). Importantly, the identification of new intermediates was not only useful to clarify the attacking sites of the molecular ozone or radicals, but also meaningful for the establishment of the degradation pathway of BZA.

In conclusion, BZA degradation pathway was as follows: (1) the molecular ozone attacks to form primary ozonides, and then, after the benzene ring-opening, to generate the aldehyde and carboxylic acid species; (2) the electrophilic substitution with HO· to form hydroxylation compounds with the benzene ring-opening and triazole ring-opening; (3) the release of N from the triazole ring to generate species with amino groups and nitro groups.

3.4. Reactive oxygen species (ROS) identification

Ozone decomposition in reactions w/o BZA is shown in Fig. 4(A) and (B). In the absence of BZA, [dissolved ozone] was about 1.0 mg/L and decreased inapparently. The consumption of ozone increased in the presence of LCO and reached 24% decomposition at 15 min. A continuous consumption of dissolved ozone with CN was observed in the

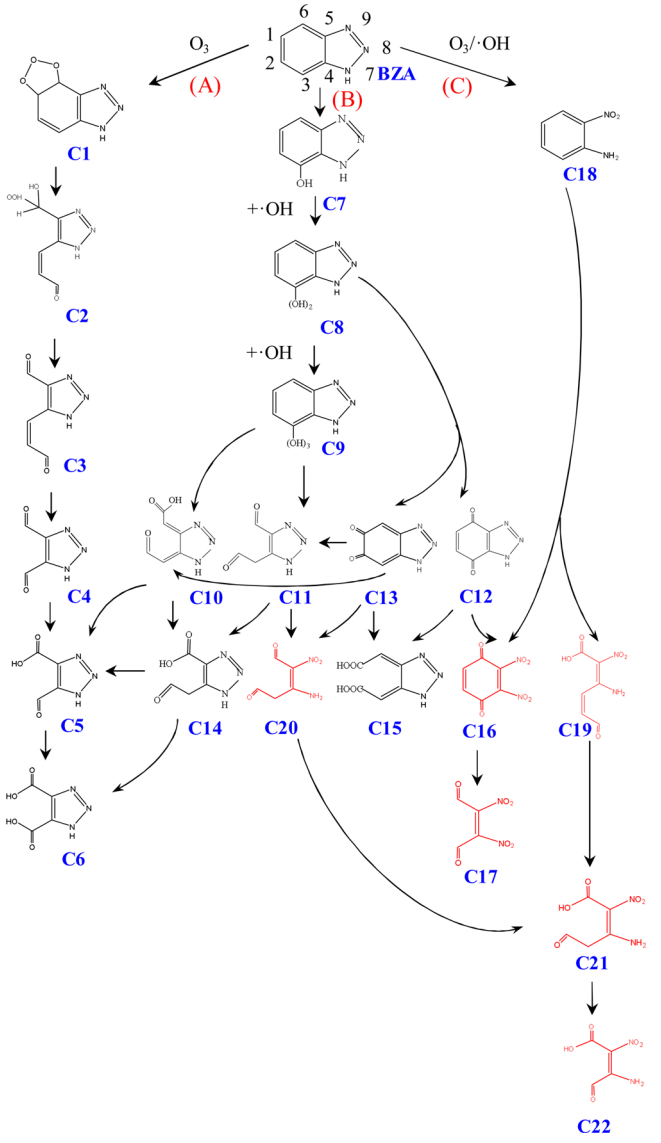

Fig. 3. Proposed transformation pathways for BZA in catalytic ozonation.

first 30 min and the consumption of ozone was 25% at 30 min. Additionally, the dissolved ozone was consumed more rapidly with the addition of 0.5-CN/LCO. A significant enhancement in ozone consumption was observed in the presence of BZA (Fig. 4(B)), which might be due to the molecular ozone oxidation on the benzene ring or –N = N– moiety of BZA. The presence of LCO and CN increased the decomposition of ozone. Similarly, the consumption of ozone was the most remarkable in the presence of 0.5-CN/LCO in BZA oxidation, compared with LCO or CN. At last, 0.5-CN/LCO showed the best ability on catalytic ozone decomposition to form ROS, leading to a higher performance on BZA degradation (Fig. 2(F)).

The typical signal of DMPO-OH with four peaks with the intensity ratio of 1:2:2:1 (with hyperfine couplings $\alpha_N = \alpha_H = 14.9$ G) was observed in the sole ozonation (Fig. 4(C)) due to the reaction pH being neutral [39]. In the presence of LCO, peaks intensity of HO· increased. LCO was reported to accelerate the decomposition of ozone to produce more HO·, which facilitated the degradation of BZA [24]. Moreover, the existence of HO· was also identified in CN catalytic ozonation as an enhancement of sole ozonation, suggesting a greater generation of HO· and being different from the a previous report [40]. Song et al., reported a similar result with ours [10]. Interestingly, the presence of 0.5-CN/LCO showed a much higher intensity of HO· peaks than other reactions, suggesting that 0.5-CN/LCO accelerated the ozone molecule decomposition, to form more HO·. This was similar with result of ZnO-CN catalytic ozonation [18].

The $O_2^{\cdot -}$ (DMPO-OOH peak ($\alpha_N = 14.2$ G, $\alpha_H^{\beta} = 11.4$ G, $\alpha_H^{\gamma 1} = 1.2$ G)) was observed in an absolute ethanol solution (Fig. 4(D)). The OH^- promoted the molecular ozone decomposition to form $O_2^{\cdot -}$ in the sole ozonation (Eq. (1)) [41].

$$O_3 + OH^- \rightarrow O_2^{\cdot -} + HO_2^{\cdot} \quad (1)$$

$O_2^{\cdot -}$ was consumed by the cyclic reaction of Co^{3+}/Co^{2+} in the catalytic ozonation of BZA (Eq. (2)), as reported in our previous study [24], leading to the decrease of the peak intensity in the presence of LCO.

$$Co^{3+} + O_2^{\cdot -} \rightarrow Co^{2+} + O_2 \quad (2)$$

After the combination of CN/LCO, the peak intensity of $O_2^{\cdot -}$ also decreased more significantly, which suggested the introduction of CN promoted the cyclic reaction of Co^{3+}/Co^{2+}.

As an important intermediate ROS, $^1O_2$ is able to be formed though the reaction of HO· and $O_2^{\cdot -}$ (Eq. (3)) [42], which was identified in this study using TEMP as the quencher (Fig. 4(E)).

$$HO\cdot + O_2^{\cdot -} \rightarrow {}^1O_2 + OH^- \quad (3)$$

The peak intensity of $^1O_2$ decreased in the addition of LCO, which may due to the consumption of $O_2^{\cdot -}$ by Co^{3+}/Co^{2+} cyclic reaction (Eq. (2)) [24], resulting in a decreased intensity of $^1O_2$. The introduction of CN improved the formation of $^1O_2$, which indicated a greater decomposition of ozone (Fig. 4(A)) in the presence of CN and generated more HO· and $O_2^{\cdot -}$ (Fig. 4(C) and (D)) that promoted the generation of intermediate $^1O_2$. Much more $^1O_2$ was formed in the addition of 0.5-CN/LCO. The faster ozone decomposition by 0.5-CN/LCO (Fig. 4(A)) and more generation of ROS (Fig. 4(C) and (D)) can be attributed to much higher intensity of $^1O_2$.

H_2O_2 will be formed in ozonation through the reaction between molecular ozone and an organic compound with olefinic bonds [43]. In the sole ozonation, the concentration of H_2O_2 increased gradually in the first 30 min with a slight decrease (Fig. 4(F)), reaching 16.5 μmol/L at 120 min. The consumption of H_2O_2 after 30 min may due to the reduction of BrO_3^- [24]. The presence of a solid catalyst did not change the profile of [H_2O_2], but increased the formation concentration, especially for 0.5-CN/LCO, which will be discussed in Section 3.5.3.

In summary, above results clearly indicated that 0.5-CN/LCO showed fast decomposition rate on the molecular ozone, which enhanced the generation of HO· that contributed to the better BZA removal efficiency (Fig. 2(F)). The formation of $O_2^{\cdot -}$ initiated the chain reactions of ozone self-decompose, combining with the cycle reaction of Co^{3+}/Co^{2+}, which attribute to more H_2O_2 formation that promoted good bromate exhibition efficiency (Fig. 2(F)). Generated $^1O_2$ that consumed HO· and $O_2^{\cdot -}$ (Eq. (3)), also promoted the decomposition of ozone to form more ROS. Co-existence of multiple ROS accelerated the ozone decomposition chain reactions, which enhanced the performance of contaminant degradation and elimination of bromate. Additionally, the capture of ROS by the matrix will be weakened by the presence of $O_2^{\cdot -}$ and $^1O_2$, due to their lower reaction constant with matrix. The contribution of ROS in this catalytic ozonation will be discussed in Section 3.5.3.

3.5. Reaction mechanism of CN/LCO catalytic ozonation and elimination of bromate

3.5.1. Absolute heterogeneous catalytic ozonation reaction

In catalytic ozonation with 0.5-CN/LCO, the leached [La^{3+}] and [Co^{3+}] were 2.55 and 0.69 mg/L (Fig. S9(A)), respectively, which only contributed 1.85% and 1.57% of the 0.5-CN/LCO dose. However, the leached metal ions did not show any development on the performance of the sole ozonation (Fig. S9(B) and (C)). Here, the absolute

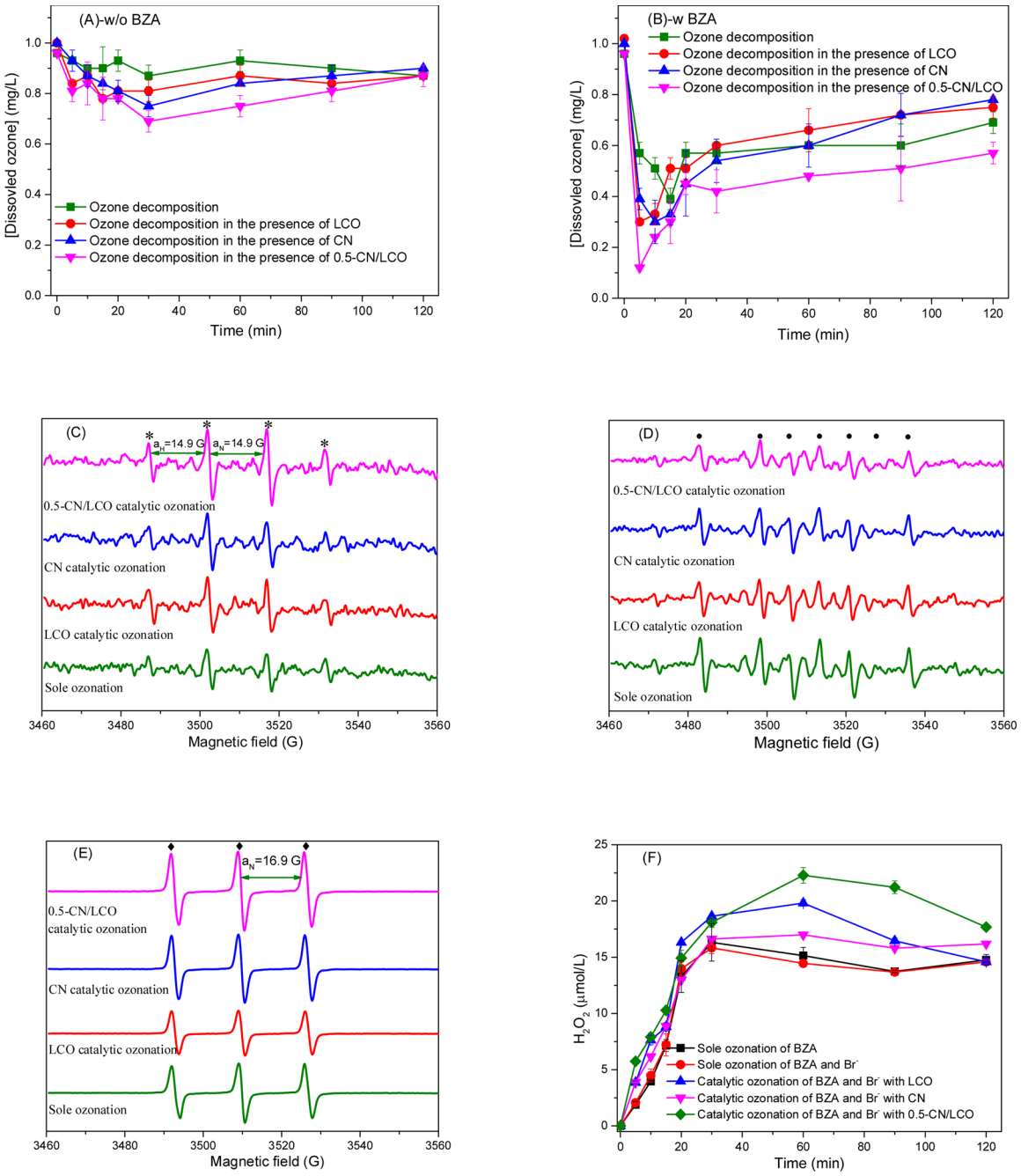

Fig. 4. Variation of [dissolved ozone] in (catalytic) ozonation without BZA (A) and with BZA (B); ESR spectra obtained using DMPO as spin-trapping regent in ultrapure water (C) and in absolute ethanol (D); using TEMP as spin-trapping regent (E); [H_2O_2] formed in different reactions (F).

heterogeneous catalysis reaction with 0.5-CN/LCO was confirmed. This was different from literatures as the homogeneous reaction achieved mineralization efficiency due to Fe^{3+} leaching from Fe-MCM-48 [44] or oxalic acid degradation ability owing to the leaching of manganese ions in $LaMnO_3$ [45]. The contribution of homogeneous reaction was not stable and metal active component leaching will decrease the usage life of the solid catalyst; however, this was not observed in this study.

3.5.2. Active centers in catalytic ozonation

XPS characterization was performed to probe the active sites and catalytic ozonation mechanism, using the variation between the fresh and the used 0.5-CN/LCO (Fig. 5 and Table S6). According to the C1 s spectrum (Fig. 5(A)), it was observed that the content of the -C-O-Co bond in 0.5-CN/LCO was reduced from 13.22% to 8.60% after being used, with the increasing relative contents of C—C and C═N—C—. The -C-O-Co bond participated in the reaction and this might be the potential active site, which was similar to the previous result where the C-O-Cu bond was the major active center in a Fenton-like reaction [15]. The decreased intensity of the —C—O—Co bond peak in catalytic ozonation was also identified according to the O1s spectrum (Fig. 5(B)), also supporting this proposed result.

According to previous report, the -C-O-Me bond is crucial for the electron transfer through cation-π interactions that offer two types of electron transfers, including π → metal cation (σ donation) and metal cation → π* (π back-donation) [9]. The metal cation would be electron-rich centers through which the π electrons shift to metal cation centers [15]. Correspondingly, electron-poor centers must be generated on the aromatic rings of CN [15]. Therefore, -C-O-Co bond, as an important

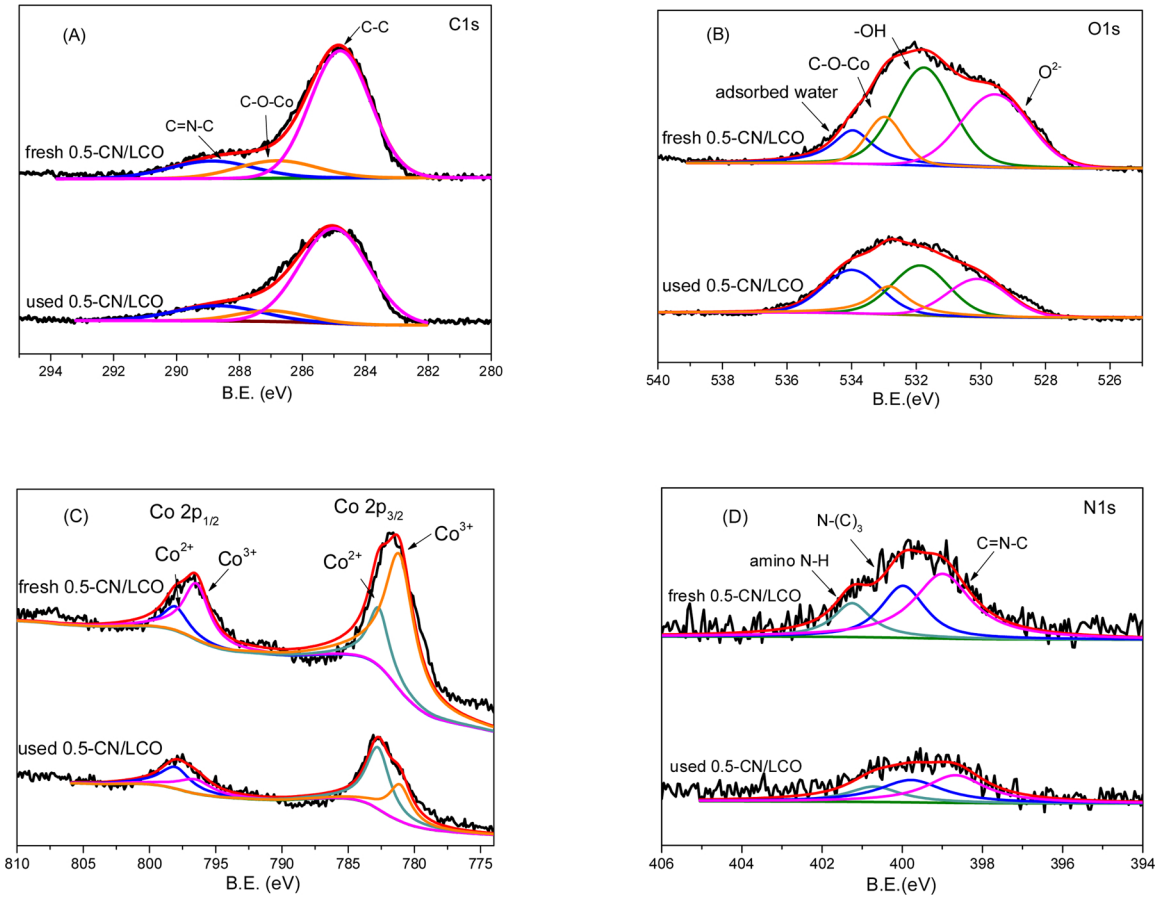

Fig. 5. XPS spectrum of fresh and used 0.5-CN/LCO, C-(A), O-(B), Co-(C) and N-(D).

active site as an electron-rich center, promoted electron transfer from π to cobalt ion and from Co ion to π* in the interlayers of 0.5-CN/LCO. The cyclic reaction of Co^{2+}/Co^{3+} led to the increase of the ratio of Co^{2+}/Co^{3+} from 0.23 to 1.69 (Fig. 5(C) and Table S7), and facilitated the decomposition of the molecular ozone [24] and Co^{3+} also might be reduced to Co^{2+} by the single electron transfer (Eq. (4)) from the electron-rich area owing to the formation of a −C−O−Co bond [9].

$$Co^{3+} + e^{-} \rightarrow Co^{2+} \quad (4)$$

According to N1 s spectrum (Fig. 5(D)), the relative C/N ratio decreased to 1.30 after catalytic ozonation (Table S7), which suggested that nitrogen vacancies participated in the process and its reduction increased the intensity of C═N−C− groups peak. The latter result was accordance with C1 s spectrum and previous research [10].

To identify the contribution of active sites in catalytic ozonation, k_{obs} of BZA degradation and different potential active sites were correlated and results are shown in Fig. 6. Results showed that k_{obs} was promoted with the increasing of the relative content of −C−O−Co (Fig. 6(A)), suggesting that the formation of -C-O-Co in the obtained novel CN/LCO plays a positive role in catalytic ozonation, which was initialized by the electron transfer between π and cobalt ion.

The improvement of k_{obs} was observed as the C/N ratio was increased (Fig. 6(B)), which indicated that nitrogen defects contributed to the catalytic ozonation. It was also reported that nitrogen defects dominated surface catalytic active sites and promoted the formation of more delocalized electrons [10]. Moreover, the electron transfer was further proved by electrochemical impedance spectroscopy (EIS). The charge-transfer resistance values were estimated according to the fitting of the Nyquist plots to an equivalent circuit diagram [46] (Fig. S10). The smallest semicircle diameter was found for 0.5-CN/LCO and the charge-transfer resistance value (0.7 kΩ) decreased dramatically compared with CN (285 kΩ) and LCO (9.1 kΩ), suggesting that 0.5-CN/LCO showed a better conductivity and a faster electron transfer performance. This will contribute the better performance of CN/LCO catalytic ozonation, interestingly.

According to a previous report, abundant hydrogen bonds in the CN framework trapped electron sites to lead to the poor interlayer electron transport [47]. Previous research attempted to break hydrogen bonds to facilitate electron transfer and to improve the performance of AOP [48]. In this study, 0.5-CN/LCO showed the lowest number of hydrogen bonds as proven by the more significant blue-shift of the peak of tri-s-triazine units in FT-IR spectrum (Fig. 2(B)). Then, the relationship between k_{obs} of BZA removal and hydrogen bonds was also investigated (Fig. 6(C)). An enhancement of k_{obs} was found with the increasing blue-shift of the peak of tri-s-triazine units, which suggested that decreasing the hydrogen bonds content would promote the BZA degradation efficiency. The presence of hydrogen bonds will block the single electrons in catalytic ozonation derived by CN/LCO, which was not similar with the general mechanism of catalytic ozonation [49].

However, it was surprising that the contribution of a surface hydroxyl group could be ignores owing to the slightly decreased surface hydroxyl group after 0.5-CN/LCO was used (from 28.07%–27.49%), which was different to the conventional knowledge of catalytic ozonation [50,51]. As shown in Fig. 6(D), the relative content of surface hydroxyl group followed the order: LCO > CN/LCO-350 > CN/LCO-400 > 0.5-CN/LCO, which was opposite to the order of the -C-O-Co relative content (Fig. 6(A)). The formation of -C-O-Co through the bonding of a cobalt atom to the deprotonated surface hydroxyl groups, led to the decrease of surface hydroxyl groups [15]. k_{obs} showed a decreasing tendency as the surface hydroxyl group content increased, indicating that the surface hydroxyl group in CN/LCO structure exhibited no contribution, rather than a negative effect. In summary, -C-

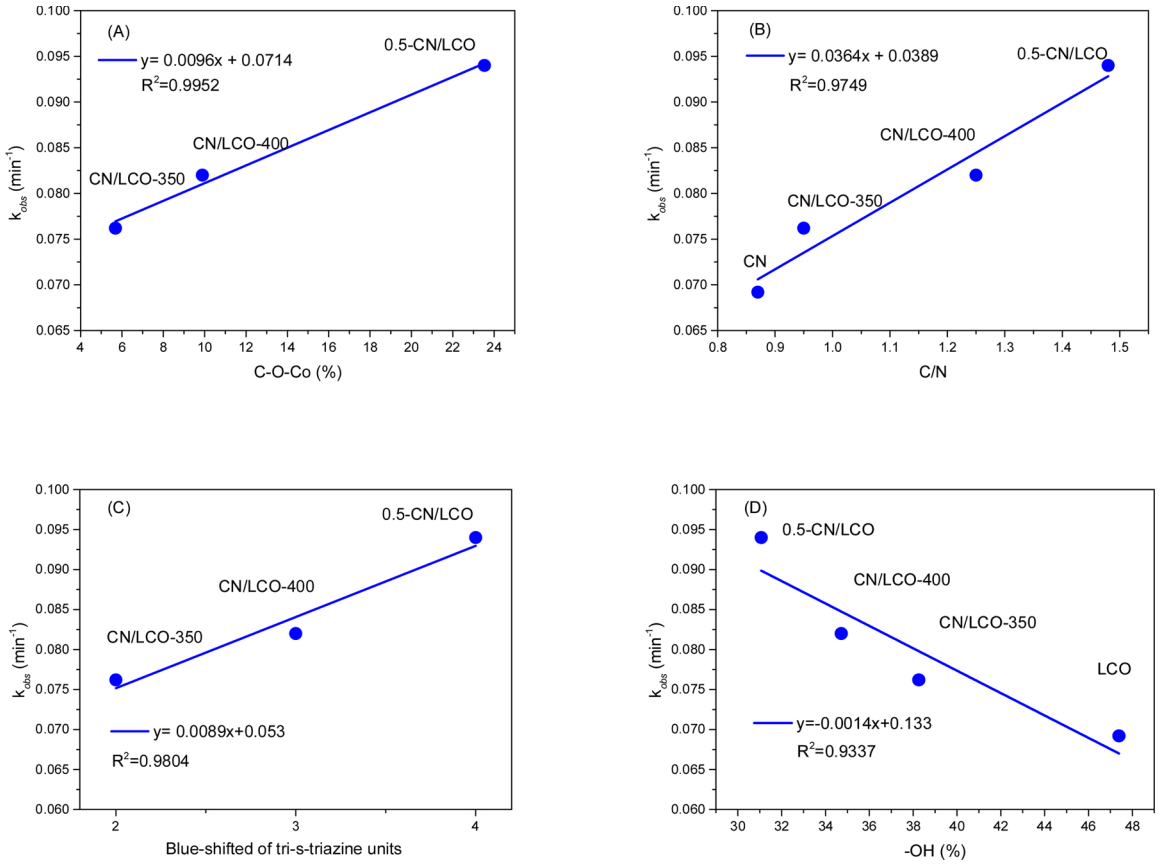

Fig. 6. Effect of -C-O-Co relative content on the degradation efficiency of BZA (A); Effect of C/N on the degradation efficiency of BZA (B); Effect of blue-shifted of FT-IR of tri-s-triazine units on the degradation efficiency of BZA (C); Relationship between surface hydroxyl group relative content and degradation efficiency of BZA (D).

O-Co and nitrogen defects were the major active sites in 0.5-CN/LCO catalytic ozonation. 0.5-CN/LCO showed the highest -C-O-Co content as an electron-rich center and more nitrogen defects that promoted electron transfer in the interlayer [15].

3.5.3. Reaction mechanism of catalytic ozonation and elimination of bromate

Based on the analysis above, the mechanism for CN/LCO catalytic ozonation is proposed in Scheme 1. It was reported that single electrons from nitrogen vacancies were easily captured by the molecular ozone to form $O_3^{\cdot -}$ (Eq. (5)) [10]. Moreover, the molecular ozone was decomposed to generate $O_2^{\cdot -}$, which followed a one-step process according to the electronic interaction through the ozone molecule and electron-rich center of −C−O−Co (Eq. (6)), which was similar with the report on ZnO catalytic ozonation [52]. Then, the decomposition of ozone was triggered by OH^- to form $O_2^{\cdot -}$ and $HO_2^{\cdot}$, as shown in Eq. (7). Additionally, absorbed O_2, as an electron acceptor that has a high electronegativity, will capture the electrons from electron-rich centers to form $O_2^{\cdot -}$ [53] (Eq. (8)).

$$O_3 + e^- \rightarrow O_3^{\bullet -} \quad (5)$$

$$O_3 \xrightarrow{C-O-Co} O_2^{\bullet -} + {}^1O_2 + O_2 \quad (6)$$

$$O_3 + OH^- \rightarrow O_2^{\bullet -} + HO_2^{\bullet} \quad (7)$$

$$O_2 + e^- \rightarrow O_2^{\bullet -} \quad (8)$$

Once $O_2^{\cdot -}$ and $HO_2^{\cdot}$ are produced, they will induce a series of radical chain reactions (Eqs. (5)–(11)) to generate HO· [24].

An electron transfer cycle formed to promote more radical generation in the interlayers: (i) the formation of the -C-O-Co bond led to rich electron centers for a faster π electron transfer through the in-plane direction, which was confirmed by the consumption of the −C−O−Co bond after the reaction (Table S6); (ii) more nitrogen defects accelerated delocalized electrons generation; (iii) the transformation of electrons between electron-rich centers produced by -C-O-Co or nitrogen defects and electron-poor centers of aromatic ring also accelerated the production of HO·. Electron transfer was also verified by EIS treatment (Fig. S10), which promoted the ozone decomposition quickly in CN/LCO catalytic ozonation (Fig. 4(A) and (B)), further accelerating HO· generation according to the chain reactions (Eqs. (5)–(11)) (Fig. 4(C)), facilitating BZA degradation (Fig. 2(F)) and the mineralization ability (Fig. S5(B)).

$$O_2^{\bullet -} + O_3 \rightarrow O_3^{\bullet -} + O_2 \quad (9)$$

$$O_3^{\bullet -} + H_2O \rightarrow HO_3^{\bullet} + OH^- \quad (10)$$

$$HO_3^{\bullet} \rightarrow O_2^{\bullet -} + HO\cdot \quad (11)$$

In CN/LCO catalytic ozonation, a better elimination of BrO_3^- formation was observed (Fig. 2(F) and Fig. S5), which may due to the faster electron transformation that accelerated the generation of H_2O_2 (Fig. 4(F)) (Eq.s (12)–(13)). Surface Co^{3+} could be reduced by $O_2^{\cdot -}$ and single electrons (Eqs. (2) and (4)), leading to the significant increase of the Co^{2+}/Co^{3+} ratio (0.23–1.69 in Table S6), which was the evidence of more consumption of $O_2^{\cdot -}$ (Fig. 4(D)). Moreover, the electron transmission promoted the cyclic reaction between Co^{2+}/Co^{3+} and further facilitated H_2O_2 formation, which reduced more BrO_3^- to HOBr/OBr^-, and the details are shown in Fig. S11 and Text S9.

$$HO_2^{\bullet} \rightarrow O_2^{\bullet -} + H^+ \quad (12)$$

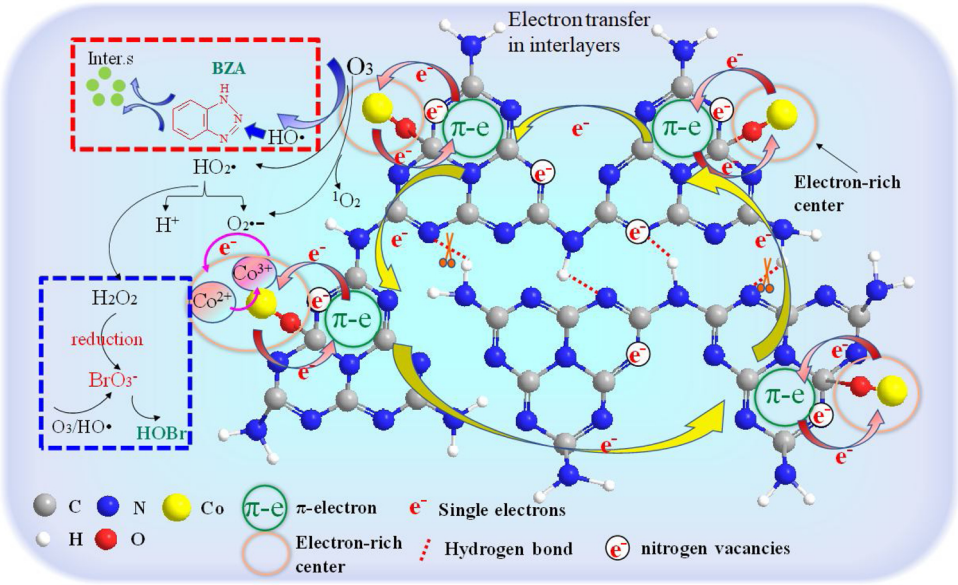

Scheme 1. Reaction mechanism of catalytic ozonation with 0.5-CN/LCO.

$$HO_2^{\bullet} + HO_2^{\bullet} \rightarrow O_2 + H_2O_2 \quad (13)$$

Therefore, CN/LCO showed higher catalytic ozonation toward BZA degradation due to the faster electron transfer through the interlayers by −C−O−Co, nitrogen vacancies and hydrogen bonds. Moreover, Co^{3+} was reduced to Co^{2+} by $O_2^{\bullet -}$ or by capturing electrons from electron-rich centers, which simultaneously accelerated the formation of H_2O_2 and the reduction of BrO_3^- to HOBr/OBr^-.

4. Conclusions

(1) CN/LCO enhanced the performance of catalytic ozonation, which achieved better BZA degradation through more production of HO·. Furthermore, CN/LCO showed remarkable elimination on toxic by-products bromate synchronously due to the generation of more H_2O_2.

(2) The formation of the -C-O-Co bond and more nitrogen vacancies promoted the generation of more delocalized electrons, which promoted the decomposition of molecular ozone to produce more HO·, rather than the general ozone decomposition pathway in catalytic ozonation to a surface hydroxyl group. Moreover, electron transfer was found to be the dominant factor in catalytic ozonation. Bonds of -C-O-Co promoted electron transfer between π-e and cobalt ion. A low number of hydrogen bonds in CN/LCO accelerated the charge transfer due to less electron trap sites along the in-plane direction. Then a large electronic recycling system along the in-plane direction was formed, which also facilitated the reduction of BrO_3^- owing to the faster cyclic reaction between Co^{3+}/Co^{2+} and more H_2O_2 formation.

(3) In this study, the possibility of catalyst design to synchronously degrade micro-pollutants and inhibit bromate was proposed. Based on CN, more nitrogen vacancies would form through the doping with a metal material, which might bring more structural defects and delocalized electrons. Metal heteroatoms doped with CN through an oxygen atom of surface hydroxyl group achieved a chemical combination that promoted electron transfer. Moreover, this may also break hydrogen bonds to decrease electron traps. The roles of defect sites and single electrons, due to the doping with metal heteroatoms, may contribute to a better micro-contaminant degradation. For the elimination of bromate, a multi-valent metal catalyst is a better choice. The cyclic reaction between multi-valent metal ions would accelerate the bromate inhibition.

Acknowledgement

This work was carried out with the support of the Fundamental Research Funds for the Central Universities (No. 2016ZCQ03), the National Natural Science Foundation of China (No. 51878047, 51578520 and 51378063), Beijing Natural Science Foundation (No. L160006 and L182027) and Open Project of State Key Laboratory of Urban Water Resource and Environment, Harbin Institute of Technology (No. HCK201709).

Appendix A. Supplementary data

Supplementary material related to this article can be found, in the online version, at doi:https://doi.org/10.1016/j.apcatb.2019.05.019.

References

[1] J. Wu, T. Su, Y. Jiang, X. Xie, Z. Qin, H. Ji, Appl. Surf. Sci. 412 (2017) 290–305.
[2] T. Gopi, G. Swetha, S. Chandra Shekar, C. Ramakrishna, B. Saini, R. Krishna, P.V.L. Rao, Catal. Commun. 92 (2017) 51–55.
[3] J.M. Cho, S.-W. Kwak, H. Aqoma, J.W. Kim, W.S. Shin, S.-J. Moon, S.-Y. Jang, J. Jo, Org. Electron. 15 (2014) 1942–1950.
[4] O. Turkay, H. Inan, A. Dimoglo, Sep. Purif. Technol. 134 (2014) 110–116.
[5] Q. Bao, K.S. Hui, J.G. Duh, J. Environ. Sci. (China) 50 (2016) 38–48.
[6] G. Márquez, E.M. Rodríguez, M.I. Maldonado, P.M. Álvarez, Sep. Purif. Technol. 136 (2014) 18–26.
[7] F. Qi, Z. Chen, B. Xu, Z. Xu, Journal of J. Water Supply Res. T. 57 (2008) 427–434.
[8] Y. Liu, X. Li, J. Liu, C. Shi, A. Zhu, Chin. J. Catal. 35 (2014) 1465–1474.
[9] N. Jiang, L. Lyu, G. Yu, L. Zhang, C. Hu, J. Mater. Chem. A 6 (2018) 17819–17828.
[10] Z. Song, Y. Zhang, C. Liu, B. Xu, F. Qi, D. Yuan, S. Pu, Chem. Eng. J. 357 (2019) 655–666.
[11] Y. Wang, H. Cao, L. Chen, C. Chen, X. Duan, Y. Xie, W. Song, H. Sun, S. Wang, Appl. Catal. B 229 (2018) 71–80.
[12] G. Li, X. Nie, J. Chen, Q. Jiang, T. An, P.K. Wong, H. Zhang, H. Zhao, H. Yamashita, Water Res. 86 (2015) 17–24.
[13] G. Li, X. Nie, Y. Gao, T. An, Appl. Catal. B 180 (2016) 726–732.
[14] W. Wang, G. Li, D. Xia, T. An, H. Zhao, P.K. Wong, Environ. Sci.: Nano 4 (2017) 782–799.
[15] L. Lyu, D. Yan, G. Yu, W. Cao, C. Hu, Environ. Sci. Technol. 52 (2018) 4294–4304.
[16] J. Ma, Q. Yang, Y. Wen, W. Liu, Appl. Catal. B 201 (2017) 232–240.
[17] X. Yuan, R. Xie, Q. Zhang, L. Sun, X. Long, D. Xia, Sep. Purif. Technol. 211 (2019) 823–831.
[18] X. Yuan, S. Duan, G. Wu, L. Sun, G. Cao, D. Li, H. Xu, Q. Li, D. Xia, Appl. Catal. A Gen. 551 (2018) 129–138.
[19] X. Yuan, W. Qin, X. Lei, L. Sun, Q. Li, D. Li, H. Xu, D. Xia, Chemosphere 205 (2018) 369–379.
[20] N.H.S. Javadi, M. Baghdadi, N. Mehrdadi, M. Mortazavi, J. Environ. Chem. Eng. 6 (2018) 6421–6430.
[21] Y.S. Liu, G.G. Ying, A. Shareef, R.S. Kookana, Water Res. 45 (2011) 5005–5014.

[22] Walter Giger, Chirstina Schaffner, H.-P. Kohler, Environ. Sci. Technol. 40 (2006) 7186–7192.
[23] Y. Zhang, C. Liu, B. Xu, F. Qi, W. Chu, Appl. Catal. B 199 (2016) 447–457.
[24] Y. Zhang, Y. Xia, Q. Li, F. Qi, B. Xu, Z. Chen, Sep. Purif. Technol. 197 (2018) 261–270.
[25] L. Cui, X. Ding, Y. Wang, H. Shi, L. Huang, Y. Zuo, S. Kang, Appl. Surf. Sci. 391 (2017) 202–210.
[26] J. Chandradass, H. Kim, F.W.Y. Momade, Adv. Powder Technol. 25 (2014) 1834–1838.
[27] N. Chidhambaram, K. Ravichandran, Mater. Lett. 207 (2017) 44–48.
[28] Y. Wu, H. Wang, W. Tu, Y. Liu, Y.Z. Tan, X. Yuan, J.W. Chew, J. Hazar. Mater. 347 (2018) 412–422.
[29] X. Rong, F. Qiu, J. Rong, J. Yan, H. Zhao, X. Zhu, D. Yang, J. Solid State Chem. 230 (2015) 126–134.
[30] C.-W. Tang, C.-B. Wang, S.-H. Chien, Thermochim. Acta 473 (2008) 68–73.
[31] O.V. Komova, V.I. Simagina, S.A. Mukha, O.V. Netskina, G.V. Odegova, O.A. Bulavchenko, A.V. Ishchenko, A.A. Pochtar, Adv. Powder Technol. 27 (2016) 496–503.
[32] H. Lan, L. Li, X. An, F. Liu, C. Chen, H. Liu, J. Qu, Appl. Catal. B 204 (2017) 49–57.
[33] Q. Xu, C. Jiang, B. Cheng, J. Yu, Dalton Trans. 46 (2017) 10611–10619.
[34] J. An, G. Zhang, R. Zheng, P. Wang, J. Environ. Sci. (China) 48 (2016) 218–229.
[35] Fernando J. Beltrán, Pablo Pocostales, Pedro Alvarez, J.F. García-Araya, O. Gimeno, Ozone: Sci. Eng. (2014) 230–237.
[36] D.B. Mawhinney, B.J. Vanderford, S.A. Snyder, Environ. Sci. Technol. 46 (2012) 7102–7111.
[37] A.G. Asimakopoulos, L. Wang, N.S. Thomaidis, K. Kannan, Environ. Int. 59 (2013) 274–281.
[38] E. Borowska, E. Felis, J. Kalka, Chem. Eng. J. 304 (2016) 852–863.
[39] M. Feng, R. Qu, X. Zhang, P. Sun, Y. Sui, L. Wang, Z. Wang, Water Res. 85 (2015) 1–10.
[40] J. Xiao, Y. Xie, H. Cao, Y. Wang, Z. Guo, Y. Chen, Carbon 107 (2016) 658–666.
[41] Y. Guo, B. Xu, F. Qi, Chem. Eng. J. 287 (2016) 381–389.
[42] Y. Wang, D. Cao, X. Zhao, Chem. Eng. J. 328 (2017) 1112–1121.
[43] Y. Guo, Z. Song, B. Xu, Y. Li, F. Qi, J.-P. Croue, D. Yuan, J. Hazar. Mater. 344 (2018) 1229–1239.
[44] X. Li, W. Chen, Y. Tang, L. Li, Chemosphere 206 (2018) 615–621.
[45] C.A. Orge, J.J.M. Órfão, M.F.R. Pereira, B.P. Barbero, L.E. Cadús, Appl. Catal. B 140–141 (2013) 426–432.
[46] S. Zhu, X. Huang, F. Ma, L. Wang, X. Duan, S. Wang, Environ. Sci. Technol. 52 (2018) 8649–8658.
[47] W. Iqbal, B. Qiu, Q. Zhu, M. Xing, J. Zhang, Appl. Catal. B 232 (2018) 306–313.
[48] H. Ou, L. Lin, Y. Zheng, P. Yang, Y. Fang, X. Wang, Adv. Mater. 29 (2017).
[49] Y. Wang, W. Yang, X. Yin, Y. Liu, J. Environ. Chem. Eng. 4 (2016) 3415–3425.
[50] F. Qi, B. Xu, Z. Chen, J. Ma, D. Sun, L. Zhang, Water Environ. Res. 81 (2009) 2411–2419.
[51] F. Qi, Z. Chen, B. Xu, J. Shen, J. Ma, C. Joll, A. Heitz, Appl. Catal. B 84 (2008) 684–690.
[52] S. Zhang, X. Quan, D. Wang, Environ. Sci. Technol. 52 (2018) 8701–8711.
[53] Y. Ren, H. Zhang, H. An, Y. Zhao, J. Feng, L. Xue, T. Luan, Z. Fan, J. Colloid Interface Sci. 526 (2018) 347–355.